ELSEVIER

Journal of Non-Crystalline Solids 185 (1995) 240–248

JOURNAL OF NON-CRYSTALLINE SOLIDS

Relationship between optical transparency and nanostructural features of silica aerogels ☆

A. Emmerling *, R. Petricevic, A. Beck, P. Wang, H. Scheller, J. Fricke

Physikalisches Institut der Universität, Am Hubland, D-97074 Würzburg, Germany

Received 18 September 1994

Abstract

Silica aerogels are considered to be of great promise for use in transparent thermal insulation systems in solar architecture. The optical transparency of these highly porous materials is influenced by the reaction parameters upon preparation and the precursor used. Previously it was shown that the specific extinction due to bulk scattering decreases both with increasing macroscopic density and increasing pH-value of the sol–gel starting solution. Recently, it was also found that within the measurement accuracy the light scattering intensity of the aerogel bulk equals the extrapolated small-angle X-ray scattering intensity towards scattering angle zero if both types of measurement are performed with respect to an absolute scale. In the meantime, ultra small-angle X-ray scattering measurements have been performed in order to close the gap in momentum space between light and conventional small-angle X-ray scattering. As a result it can be stated that the nearly isotropic (Rayleigh) scattering is caused by the same nanostructural inhomogeneities of the aerogel network which lead to the characteristic small-angle scattering pattern. As a consequence, the amount of isotropically scattered light and thus the optical extinction can be directly related to a quantity called the correlation volume. For a variety of silica aerogels, it is shown how the latter depends on the nanostructural features of the gel network, such as average particle size, interparticle arrangement, pore diameter and an ordering parameter, which accounts for concentration effects.

1. Introduction

Aerogels are sol–gel-derived, supercritically dried materials with extraordinary properties resulting from their highly porous nanostructure [1]. In addition, silica aerogels are transparent in the visible region which makes them promising materials for transparent thermal insulation in solar architecture [2,3]. The use of monolithic aerogels in superinsulating windows, however, requires a considerable improvement of the transparency.

Since the absorption of silica is negligible in the visible range, the extinction of light results solely from scattering. Two different sources of light scattering (LS) in aerogels have been found [4]: scattering due to micrometer-size imperfections of the external aerogel surface, which is the reason for the slightly fuzzy appearance of objects viewed through a piece of aerogel [5], and scattering from the nanoporous aerogel network. Since the inhomogeneities of the aerogel network are much smaller

☆ Presented at the 4th International Symposium on Aerogels, Berkeley, CA, USA, 19–21 September 1994.

* Corresponding author. Tel: +49-931 888 5761. Telefax: +49-931 888 5158. E-mail: emmerling@physik.uni-wuerzburg.de.

SSDI 0022-3093(95)00021-6

than the light wavelengths, nearly isotropic light (Rayleigh) scattering is expected and observed. This bulk scattering, I_B, was shown to vary drastically upon the silica content and catalyst concentration of the sol–gel starting solution for series of one- or two-step reacted tetramethoxy silane (TMOS) aerogels [6]. The highest transparency has been achieved for strongly base-catalyzed aerogels having a density of about 200 kg/m^3 [6–8]. Aerogels prepared from aqueous sodium silicate (waterglass) solutions, which have been assigned for use in large-scale commercial applications because of the cheap, non-flammable and non-hazardous precursor, show a hemispherical transmittance in the visible range of only 50–60% for a 20 mm thick granular layer [9].

Recently we showed that the optical transparency can be correlated to the structural build-up of the gel network as derived from small-angle X-ray scattering (SAXS) measurements [10]. This statement was deduced from the equality of I_B and the extrapolated zero-angle SAXS intensity $I_X(\theta \to 0)$. To corroborate this hypothesis, ultra small-angle X-ray scattering (USAXS) experiments have been performed to close the gap in scattering vector between LS and conventional SAXS.

2. Theory

To be able to compare LS and SAXS curves both intensities have to be reduced to the same scale. Generally, the intensity measured in a scattering experiment is given by (see, for example, Ref. [11])

$$I(q) = I_0 T V \frac{\mathrm{d}\Sigma}{\mathrm{d}\Omega} \Delta\Omega w = f \frac{\mathrm{d}\Sigma}{\mathrm{d}\Omega}, \tag{1}$$

where I_0 is the incident intensity, T is the sample transmission, V is the illuminated volume, $\Delta\Omega$ and w are the solid angle and sensitivity of the detector, respectively, and $q = (4\pi/\lambda)\sin(\theta/2)$ is the scattering vector, with λ being the wavelength used and θ the scattering angle. The volume-specific scattering cross-section

$$\frac{\mathrm{d}\Sigma}{\mathrm{d}\Omega} = \langle \delta^2 \rangle \int_0^\infty 4\pi r^2 \gamma(r) \frac{\sin qr}{qr}\, \mathrm{d}r = \langle \delta^2 \rangle V_c(q) \tag{2}$$

depends on the mean square fluctuation (MSF) of the scattering length density $\langle \delta^2 \rangle = \langle (\delta(r) - \langle \delta \rangle)^2 \rangle$ and the integral over the correlation function, $\gamma(r)$, which contains the information of the geometric build-up of the sample. It is hereby assumed that the samples under investigation are statistically isotropic, i.e., $\gamma(\boldsymbol{r}) = \gamma(r)$, and the scattering pattern is radially symmetric ($I(\theta, \varphi) = I(\theta)$). The polarization factor $(1 + \cos^2\theta)/2$ approaches unity in the case of small-angle scattering; in other cases, only the component of scattered light perpendicular to the scattering plane is considered. In the following, the integral term is abbreviated by $V_c(q)$, i.e., a q-dependent volume in which coherent scattering takes place.

In the case of X-ray scattering (X), $\langle \delta_X^2 \rangle$ is given by the product of the square of the classical electron radius, r_e, and the MSF in electron density $\langle \eta_X^2 \rangle$. For a two-phase media system with a zero-density pore space such as aerogels, the MSF can be written as

$$\langle \delta_X^2 \rangle = r_e^2 \langle \eta_X^2 \rangle = \left(r_e \frac{ZN_A}{M_v} \rho_s \right)^2, \tag{3}$$

with ZN_A being the number of electrons per mole, M_v the molar mass and ρ_S the mass density of the aerogel backbone. For light scattering in the Rayleigh–Gans approximation [12], a similar relationship is obtained:

$$\langle \delta_L^2 \rangle = \frac{\pi^2}{\lambda^4} \langle \eta_L^2 \rangle, \tag{4}$$

where $\langle \eta_L^2 \rangle$ denotes the MSF of the dielectric constant. For a two-phase media system $\langle \eta_L^2 \rangle$ can be calculated from

$$\langle \eta_L^2 \rangle = \phi(\varepsilon_s - \varepsilon)^2 + (1 - \phi)(\varepsilon - 1)^2, \tag{4a}$$

with ε_s being the dielectric constant and $\phi = \rho/\rho_s$ the volume fraction of the solid phase; ρ is the apparent macroscopic density of the aerogel. The average dielectric constant of the porous medium, ε, can be obtained from the Clausius–Mosotti relation using the values for non-porous vitreous silica [13]:

$$N\alpha = \frac{\varepsilon - 1}{\varepsilon + 2} = \phi \frac{\varepsilon_s - 1}{\varepsilon_s + 2} = \frac{\rho}{\rho_v} \frac{\varepsilon_v - 1}{\varepsilon_v + 2}, \tag{4b}$$

where α denotes the molecular polarizability and N the number density of dipoles; $\rho_V = 2190$ kg/m^3 and $\varepsilon_V = 2.13$ are the values for non-porous vitreous silica. Using Eq. (4b), ϕ and ε_S in Eq. (4a) can be replaced by ρ/ρ_V and ε_V.

The optical extinction, E, is related to the differential cross-section and the measured light scattering cross-section via

$$E = \int_{4\pi} \frac{d\Sigma}{d\Omega}(q) \frac{1+\cos^2(\theta)}{2} d\Omega; \quad (5a)$$

an auxiliary extinction, E^*, can be calculated from

$$E^* = \int_{4\pi} I_L(q) \frac{1+\cos^2(\theta)}{2} d\Omega. \quad (5b)$$

The ratio, $f = E^*/E$, contains all (unknown) experimental parameters (see Eq. (1)). By determination of the extinction, E, for instance from a measurement of the directional–directional transmission of the sample ($T_{dd} = e^{-Ed}$, with sample thickness, d) and calculation of the auxiliary extinction, E^*, from the scattered intensity, $I_L(q)$, measured in arbitrary units, it is thus possible to obtain the correlation volume of the sample:

$$V_{C,L}(q) = \frac{1}{\langle \delta_L^2 \rangle} \frac{d\Sigma_L}{d\Omega}(q) = \frac{1}{\langle \delta_L^2 \rangle} \frac{E}{E^*} I_L(q). \quad (6)$$

Using the invariant

$$Q = \int_0^\infty q^2 \frac{d\Sigma}{d\Omega}(q)\, d\Omega = 2\pi^2 \langle \delta_X^2 \rangle \quad (7)$$

together with Eq. (2), the X-ray scattering intensity can also be reduced to a q-dependent correlation volume,

$$V_{C,X}(q) = \frac{2\pi^2}{Q} \frac{d\Sigma}{d\Omega}(q), \quad (8)$$

even if $I_X(q)$ is measured in arbitrary units.

3. Experimental

3.1. Sample preparation

To study the influence of the nanostructure on the optical extinction, the following samples have been investigated: silica aerogels, having almost constant apparent density but being differently catalyzed, were prepared by hydrolysis and condensation of tetramethoxysilane (TMOS) with a stoichiometric amount of water [14]. The target density of the gel was adjusted by an additional amount of methanol; ammonia was used as a catalyst. The catalyst concentration is written as a pseudo pH-value, i.e., pH = 14 − log[NH_4OH]. A waterglass gel was prepared by replacing TMOS by the equivalent amount of sodium silicate solution; water and sulphuric acid were used as excess solvent and catalyst, respectively. In addition, a Na-doped TMOS gel was produced by adding 0.1 mol% Na_2SO_4 to the TMOS starting solution. The sample designation reads as follows: $X - Y/Z$, where X stands for the precursor (T is TMOS, T* is Na-doped TMOS and W is waterglass), Y gives the pH-value and Z the macroscopic target density in kg/m^3. After about 1 week of aging, all gels were supercritically dried with respect to methanol; the aqueous solvent of the W-gel was exchanged for methanol prior to drying. Shrinking of all samples during aging and drying led to a final macroscopic density of about 200 kg/m^3. Granular materials having comparable densities have also been investigated: SiO_2-aerogel granules provided by BASF, Ludwigshafen, Germany, which are also prepared from waterglass, and granules prepared from a condensed silica precursor via a two-step reaction at Lawrence Livermore National Laboratory (LLNL) [15].

3.2. Experimental

A polar nephelometer was employed to probe the angular distribution of the scattered light intensity. A chopped and polarized He–Ne laser beam was used as a light source ($\lambda = 633$ nm); the scattered intensity was detected with a photomultiplier mounted on a goniometer. The accessible range of q was 0.001–0.02 nm^{-1}. For a detailed description of corrections due to the experimental arrangement and the sample geometry, see Ref. [13]; the experimental set-up for separating surface and bulk scattering contributions is given in Ref. [4]. A commercial double-beam spectrometer (Perkin–Elmer Lambda 9) was employed to determine the optical extinction via trans-

mission measurements in the wavelength range from 200 to 800 nm [8].

SAXS measurements were carried out with a Kratky camera (KCLC/2) mounted on a desktop X-ray generator (Philips PW1830/40) with a Cu anode ($\lambda_{K\alpha} = 0.154$ nm). A one-dimensional position-sensitive detector (Raytech) with 70 μm resolution was used to register the scattering profile at a distance of 245 mm from the sample position. A pinhole primary beam profile (0.08×0.5 mm^2) was used in order to neglect slit smearing corrections. Owing to the strong scattering power of aerogels, the measurement time could be limited to about to 3–4 h. With this equipment, a range of q from 0.07 to 4 nm^{-1} could be covered.

Further SAXS measurements were performed at the JUSIFA beam line [16] of the storage ring DORIS III at HASYLAB/DESY (Hamburg) using point collimation (0.5×0.5 mm^2), an X-ray wavelength of 0.15 nm and two different sample–detector distances (935 and 3635 mm); thus a range of q from 0.08 to 6 nm^{-1} was covered. The high intensity of the incident synchrotron radiation as well as the use of a two-dimensional position-sensitive detector (0.8×0.8 mm^2 pixel size) resulted in excellent signal-to-noise ratios within short measurement times.

Ultra small-angle X-ray scattering measurements were also performed at HASYLAB using the beamline BW4 [17]. Owing to the small pixel size of the 2D detector (0.4×0.4 mm^2), the accessible range of q is 0.01–0.7 nm^{-1} at a wavelength of 0.14 nm and a sample–detector distance of 12.45 m.

For all X-ray scattering measurements, thin slices of about 1 mm thickness were cut in order to guarantee a defined scattering volume. A monitor counter was used to eliminate temporal fluctuations of the primary beam intensities. The final calibration was performed by measuring a reference sample (glassy carbon) with a known scattering cross-section. Therefore, USAXS and SAXS intensities could be independently reduced to volume-specific cross-sections before the invariant of the composed scattering curve was calculated.

4. Results

Fig. 1 represents the reduced X-ray (SAXS,USAXS) scattering intensities of three one-

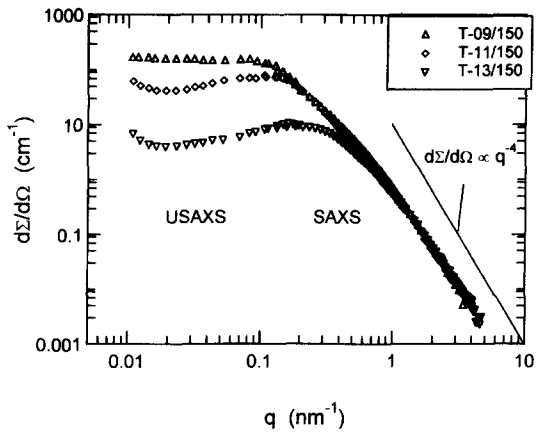

Fig. 1. Volume-specific SAXS and USAXS cross-sections as a function of the momentum transfer for the three differently catalyzed TMOS aerogels of similar macroscopic density ($\rho \approx 230$ kg m^{-3}). A perfect agreement of both type of measurements is obtained in the overlap range ($q = 0.08$–0.7 nm^{-1}). For a better visibility, only every fourth datapoint of the USAXS data below $q = 0.04$ nm^{-1} and every sixth above $q = 0.04$ nm^{-1} are shown, respectively.

step reacted aerogel specimens catalysed at pH = 9, 11 and 13. An excellent agreement between both types of measurement can be observed in the overlap regime. The light scattering curves of these samples are depicted in Fig. 2. The two contributions, I_S and I_B, are shown for sample T-13/150. Using the scattering function of a statistical two-phase system [18], both parts can be fitted well, each with a different correlation length, and the surface contribution can easily be subtracted. To normalize the remaining bulk scattering, I_B, via Eq. (6), the respective bulk extinction, E_B, has to be determined. Since the surface inhomogeneities are much larger than the light wavelength used, the extinction, E_S, due to surface scattering is nearly wavelength-independent [4,6–9]. The measured extinction, E, can thus be written as

$$E(\lambda) = E_B(633\ \text{nm})(633\ \text{nm}/\lambda)^4 + E_S. \qquad (9)$$

This relationship is shown in Fig. 3. For the determination of $E_B{}^*$ via Eq. 5(b) an error of about 20% can be estimated; this is due to the incompletely measurable angular range leading to errors upon extrapolation ('thin platelet' geometry, gap between $\theta \approx 75°$ and 105° [4]). Together with experimental errors of about 5–10% from the extinction measure-

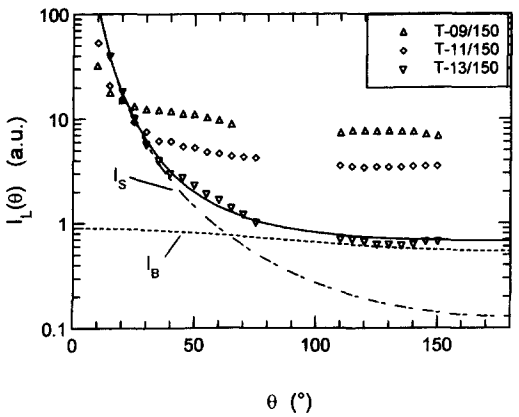

Fig. 2. Light scattering intensities of the three TMOS aerogel samples of Fig. 1. Two contributions can be observed: nearly isotropic scattering from the nanostructured aerogel bulk, I_B, (– – –), and an increasing scattering, I_S, towards smallest scattering angles due to micrometer-size inhomogeneities of the external aerogel surface (— — —) [4]. Employing a statistical two-phase media model [18] for both contributions, a separation can be achieved which is shown for sample T-13/150. The lack of data for scattering angles $\theta = 75$–$105°$ is due to the measurement geometry [4].

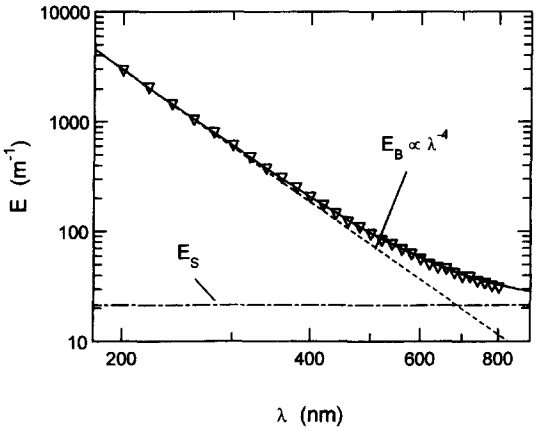

Fig. 3. Wavelength dependence of the optical extinction coefficient, E. The bulk scattering, E_B, shows the typical λ^{-4} decay (Rayleigh scattering) (– – –), whereas the surface contribution, E_S, is nearly independent of wavelength (— — —) [7,8].

ment, the accuracy of the normalization of LS amounts to about 30%. The error in the SAXS data due to calibration via the invariant Q is about 2–4%; thanks to the q^2-weighting, errors due to extrapolation can be neglected.

The combined LS and (U)SAXS curves for this pH series is represented in Fig. 4. A satisfactory agreement between $V_{C,L}(q)$ and $V_{C,X}(q)$ can be observed in the overlap region. The increase of $V_{C,L}(q)$ and $V_{C,X}(q)$ towards smallest scattering vectors is not sample-specific but depends on what part of the external surface is illuminated; fluctuations up to a factor of five have been found [4]. Table 1 contains the extinction, E_B, and the correlation volumes, $V_{C,L}(0)$ and $V_{C,X}(0)$; the structural parameters are referred to in the Discussion section.

The SAXS profiles, $V_{C,X}(q)$, of the monolithic waterglass aerogel, the two granular aerogels and, for comparison, the T-13/150 sample are depicted in Fig. 5. Although all specimens are of comparable density, strong differences can be in observed in $V_{C,X}(q \to 0)$, which is proportional to the optical extinction, E_B (see Table 1). The two-step-reacted granular aerogel is nearly as transparent as the optimum TMOS aerogel, whereas the monolithic waterglass sample exhibit a 30 times larger extinction

Table 1
Macroscopic density, ρ, mean fluctuation square, η_L^2, optical bulk extinction, E_B, at $\lambda = 633$ nm, LS and SAXS-derived correlation volumes, $V_{c,L}(0)$ and $V_{c,X}(0)$, respectively, particle radius, R, and cluster size, ξ, fractal dimension, D, and packing ratio, p, for the SiO_2 aerogels investigated

Sample	ρ (kg m^{-3})	η_L^2	E_B (m^{-1})	$V_{c,L}(0)$ (nm^3)	$V_{c,X}(0)$ (nm^3)	R (nm)	ξ (nm)	D	p
T-9/150	220	0.117	155	1719	1517	3.20	15.7	2.22	0.08
T-11/150	230	0.122	63.9	682	451	2.13	15.0	2.24	0.35
T*-11/150	240	0.126	198	2043	2094	3.4	19.4	2.25	0.14
T-13/150	234	0.123	6.97	73	32	0.96	8.4	2.02	0.45
W-5/200	220	0.117	190	2099	1784	2.28	13.7	2.33	0
BASF	200	0.107	65	503	816	1.93	11.9	2.30	0.04
LLNL	240	0.126	22.1	227	251	0.83	12.0	2.38	0.26

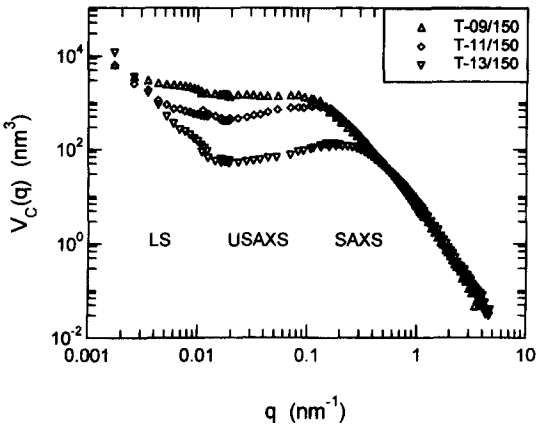

Fig. 4. Reduced LS, SAXS and USAXS intensities represented by $V_c(q)$ of three one-step-reacted TMOS aerogels with comparable apparent density ($\rho \approx 230$ kg/m^3) but different catalyst concentration. A satisfactory agreement between the light scattering intensity of the aerogel bulk and the X-ray intensity towards small scattering vectors is observed. The error bars of about 30% reflect the uncertainty due to the normalization procedure for LS; the statistical errors of the SAXS data are less then 1%. The intensity increase at smallest scattering vectors, q, is due to light scattering from large inhomogeneities at the external aerogel surface; the bulk scattering intensity can be regarded as nearly isotropic [4].

compared with the optimum TMOS aerogel. Fig. 6 contains the correlation volumes of the Na-doped T*-9/200 sample and the corresponding undoped

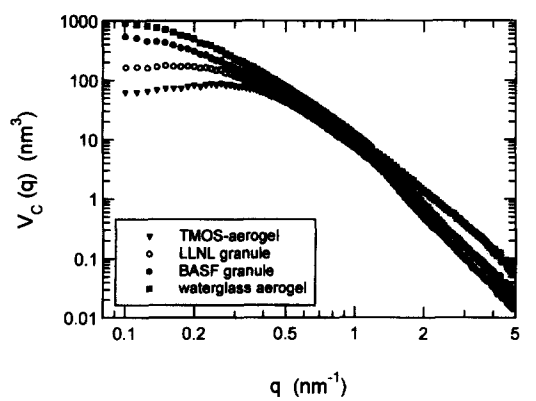

Fig. 5. Combined SAXS and USAXS correlation volumes of two aerogel granular materials, provided by BASF AG and LLNL, as well as a monolithic waterglass aerogel and the optimum transparent TMOS aerogel T-13/150. Although all aerogels are of comparable density, strongly different zero-angle scattering intensities can be observed which give rise to the large differences in transparency.

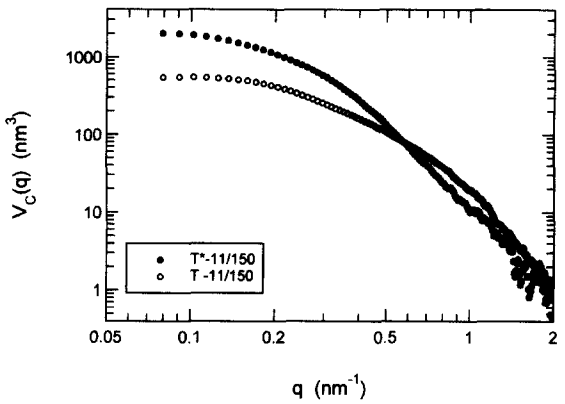

Fig. 6. SAXS correlation volumes of the TMOS aerogels T-11/150 and T*-11/150; the latter has been doped with 0.1 mol% sodium sulphate. This obviously led to an enlargement of the size parameters and therefore to increased forward scattering and optical extinction.

TMOS aerogel. Introducing sodium obviously leads to a decreased transparency.

5. Discussion

The correspondence between reduced light and small-angle X-ray scattering data shows that both types of scattering take place at the same inhomogeneities of the aerogel network, described by the normalized correlation function, $\gamma(r)$. As a consequence, the optical extinction can directly be related to the quantities of the nanostructure as determined by (U)SAXS. According to the hierarchical build-up of the aerogel network, $V_c(q)$ can be written as

$$V_c(q) = V_0 \Phi(q) S(q) P(q), \tag{10}$$

if monodisperse building blocks are assumed, with V_0 being the volume of a primary particle. Because of polydispersity, no oscillations of the scattered intensity are observed in the limiting Porod regime; the q^{-4} decay indicates smooth inner surfaces for all samples investigated. Therefore, a Debye function is suitable to approximate the particle form-factor:

$$P(q, R) = \left(1 + \frac{\sqrt{2}}{3} q^2 R^2\right)^{-2}. \tag{11}$$

The constant $\sqrt{2/3}$ was chosen to let $P(q, R)$ correspond to the form-factor of a perfect sphere at

large scattering vectors ($P \propto 4.5(qR)^{-4}$); R can then be regarded as a sphere radius. During the sol–gel process, the primary particles aggregate forming branched clusters, which are generally characterized by the mass fractal dimension, D [19]. D describes how the cluster mass scales with the cluster size ($M \propto \xi^D$) and depends on the process for cluster growth [20]. The fractal behaviour is limited to the range between cluster size, ξ, and particle radius, R, which extends over one order of magnitude in length scale for medium-density aerogels (100–200 kg/m^3). Though the fractal concept should not be overemphasized for such aerogels, the scaling of the cluster mass shows up in the structure factor, $S(q)$, which can be calculated starting off with a correlation function consisting of a power-law term and an exponential cut-off length to account for a limited maximum cluster size ($\gamma(r) \propto r^{D-3}\exp(-r/\xi)$) [21]:

$$S(q, R, \xi, D) = 1 + \frac{D\Gamma(D-1)}{(qR)^D}\left(1 + \frac{1}{(q\xi)^2}\right)^{(1-D)/2} \times \sin\left[(D-1)\tan^{-1}(q\xi)\right], \quad (12)$$

where Γ denotes the gamma-function. While $S(q)$ shows a broad crossover from the 'fractal' regime ($S(\xi^{-1} < q < R^{-1}) \propto q^{-D}$) to the constant value ($S_{(0)} = \Gamma(D+1)(\xi/R)^D$) at smallest scattering vectors, for most of the base-catalyzed aerogels a sharp crossover and even a decrease in scattered intensity towards scattering angle zero is observed. This behaviour can be ascribed to concentration effects, i.e., close packing of nearly monodisperse clusters; the maximum might then be interpreted as a Bragg peak of the spacing between neighbouring clusters. A first approximation is to treat the clusters as hard spheres which leads to a concentration factor of

$$\Phi(q, L, p) = 1/(1 + 8p\Theta(qL)), \quad (13)$$

with $\Theta(qL)$ being the scattering amplitude of a perfect sphere with radius L [22]. In the case of monodispersity, p is the packing ratio, i.e., the particle volume over the average volume available per particle. Although the clusters have an open structure and can partially penetrate each other, $\Phi(q)$ is sufficient to fit the data. The single structure functions are depicted schematically in Fig. 7 together with the resulting scattering function, $V_c(q)$. The results of fitting Eq. (10) to the experimental data are given in Table 1.

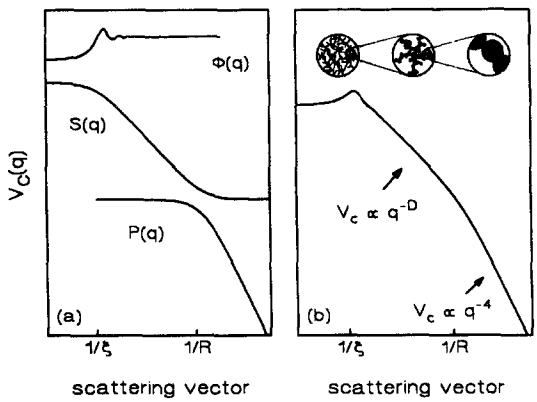

Fig. 7. (a) Schematic diagrams of the particle form-factor, $P(qR)$, the structure factor, $S(q, R, \xi, D)$, and the concentration factor, $\Phi(qL)$. (b) The correlation volume $V_c(q) \propto \Phi(q)S(q)P(q)$, which is typical for an aerogel [21]. The different structural features of the gel network (continuum–cluster–particle) show up at the corresponding scattering vectors.

If isotropic light scattering occurs (I_L = constant), E is simply proportional to $V_{C,L}(0)$:

$$E_B = (4\pi^3/\lambda^4)\langle\eta_L^2\rangle V_{C,L}(0), \quad (14)$$

which can be written according to the hierachical structure model as

$$V_C(0) = \frac{4\pi}{3}\frac{\Gamma(D+1)}{1+8p}\xi^D R^{3-D}. \quad (15a)$$

Using $\phi = (\rho/\rho_S) \approx M/V \propto (\xi/R)^D/(\xi/R)^3 = (\xi/R)^{D-3}$, two different forms of Eq. (15a) can be given:

$$V_C(0) = \frac{4\pi}{3}\frac{\Gamma(D+1)}{1+8p}R^3\phi^{D/(D-3)} \quad (15b)$$

and

$$V_C(0) = \frac{4\pi}{3}\frac{\Gamma(D+1)}{1+8p}\xi^3\phi. \quad (15c)$$

Thus it can be concluded which structural parameters should be altered to effectively improve the optical transparency: at a given macroscopic density, the

primary particle diameter, R, must be made small; the average cluster size, ξ, will then automatically decrease and vice versa (Eqs. (15b) and (15c)). Fixing the particle size and changing the density by the cluster size leads to a ρ^{-2} behaviour of the zero-angle correlation volume for $D \approx 2$, and thus to a ρ^{-1} behaviour of the bulk extinction (Eq. (14)), since the MSF of the dielectric constant is proportional to ρ for low densities (Eq. 4(a)). At constant particle size *and* density, a reduction of D from 2.1 (reaction-limited aggregation) to 1.7 (diffusion-limited growth) will decrease the forward scattered intensity (Eq. (14b)); the corresponding change in the exponent of ϕ from 2.3 to 1.4 will be more important the smaller the relative density. In addition, diffusion-limited growth seems to cause a semi-ordered state in the cluster packing, similar to that what has previously been observed for the aggregation of polysterene spheres by Carpineti and Giglio [23]. In this case the concentration factor, Φ, develops which further decreases $V_C(0)$.

The strong dependence of the extinction on particle and cluster sizes can be recognized for the pH variation (Fig. 4). Increasing the catalyst concentration decreases both size parameters. The reason for the low extinction of the two-step reacted granules is mainly due to the small particle size of the precondensed silica precursor obtained in the first reaction step. During the second step only aggregation and no growth of these primary particles takes place. At a constant density, a small particle size necessarily leads to a small average cluster size, diminishing both $V_C(0)$ and E_B. Although the primary particles of this material are smaller than that of the pH13-TMOS aerogel, it shows a higher $V_C(0)$. This results from the difference in fractal dimension, D.

On the other hand, waterglass systems consist of comparatively large particles and big clusters, causing a deteriorated transparency. Since waterglass contains a considerable amount of sodium ions, one TMOS aerogel (T-11/150) has been doped with Na_2SO_4 in order to check whether the presence of sodium might be responsible for the formation of enlarged particle (and thus cluster) diameters. Astonishingly, addition of only 0.1 mol% Na_2SO_4 is sufficient to increase the size parameters by a factor of about three and increases the extinction by one and a half orders of magnitude.

6. Conclusions

It can be explicitly shown for a variety of silica aerogels that light and X-ray scattering can be described by the same correlation function. It is therefore possible to relate the optical extinction to the nanostructural build-up of the aerogel network and to decide which structural parameters must be changed to obtain highly transparent materials. At given density: (i) the particle (and thus the cluster) diameters has to be kept small and (ii) a diffusion-limited growth process should be adjusted by suitable chemical conditions. This can be achieved by high concentrations of basic catalyst in the starting solution of one-step-reacted TMOS aerogels, or by employing a two-step reaction. The reduced transparency of waterglass systems was found to result from large particle and cluster sizes. This seems to be due to the presence of sodium ions as shown by adding sodium to TMOS solutions. At the moment it is not clear what role the sodium actually plays and which reaction steps are influenced by it. SAXS investigations of the structural development during the respective sol–gel processes might give further evidence.

The authors are grateful to the German BMFT (contract number 03M2717) for financial support, and are obliged to BASF AG and Dr L.W. Hrubesh (LLNL) for providing aerogel granules.

References

[1] J. Fricke and A. Emmerling, Aerogels – Preparation, Properties and Applications, ed. R. Reisfeld and C.K. Jorgensen, Springer Series in Structure and Bonding, Vol. 77 (Springer, Berlin, 1992) p. 37.

[2] A. Goetzberger and V. Wittwer, in: Aerogels, ed. J. Fricke, Springer Proceedings in Physics, Vol. 6 (Springer, Berlin, 1986) p. 84.

[3] Novakov, oral report, 2nd Int. Workshop on Transparent Insulation, Freiburg, 1988.

[4] P. Wang, W. Körner, A. Emmerling, A. Beck, J. Kuhn and J. Fricke, J. Non-Cryst. Solids 145 (1992) 141.

[5] A. Beck, J. Linsmeier, W. Körner, H. Scheller and J. Fricke, in: Proc. 4th Int. Symp. on Aerogels, ed. R.K. Pekala and L.W. Hrubesh, J. Non-Cryst. Solids (1995) in press.

[6] P. Wang, thesis, Universität Würzburg (1993).

[7] A. Beck, G. Popp, A. Emmerling and J. Fricke, J. Sol–Gel Sci. 2 (1994) 913.

[8] A. Beck, W. Körner, G. Popp, H. Scheller, A. Emmerling

and J. Fricke, Optical Properties of Aerogels, ISES Solar World Congress, Budapest, Aug. 23–27, 1993.
[9] A. Beck, W. Körner and J. Fricke, J. Phys. D 27 (1994) 13.
[10] A. Emmerling, P. Wang, G. Popp, A. Beck and J. Fricke, J. Phys. (Paris) IV 3 (1993) C8-360.
[11] P. Lindner and T. Zemb, eds., Neutron, X-ray and Light Scattering (North-Holland, Amsterdam, 1991).
[12] M. Kerker, The Scattering of Light (Academic Press, London, 1969).
[13] A. Beck, R. Caps and J. Fricke, J. Phys. D22 (1989) 730.
[14] C.J. Brinker and G.W. Scherer, Sol–Gel Science (Academic Press, Boston, MA, 1990).
[15] M. Tillotson and L.W. Hrubesh, J. Non-Cryst. Solids 145 (1992) 44.
[16] H.-G. Haubold, K. Gruenhagen, M. Wagener, H. Jungbluth, H. Heer, H. Rongen, G. Brandenburg, R. Moeller, P. Hiller, H. Halling, A. Pfeil and J. Matzerath, Rev. Sci. Instrum. 60 (1989) 1943.
[17] R. Gehrke, Rev. Sci. Instrum. 63 (1992) 455.
[18] P. Debye, H.R. Anderson and H. Brumberger, J. Appl. Phys. 28 (1957) 679.
[19] B.B. Mandelbrot, The Fractal Geometry of Nature (Freeman, San Francisco, 1982).
[20] D.W. Schaefer, Rev. Phys. Appl. 24-C4 (1988) 121.
[21] J. Teixeira, J. Appl. Crystallogr. 21 (1988) 781.
[22] D. Posselt, J.S. Pedersen and K. Mortensen, J. Non-Cryst. Solids 145 (1992) 128.
[23] M. Carpineti and M. Giglio, Phys. Rev. Lett. 70 (1993) 3828.